Materials Letters 234 (2019) 196–200

Contents lists available at ScienceDirect

Materials Letters

journal homepage: www.elsevier.com/locate/mlblue

# Effect of post-process heat treatment on microstructure and properties of selective laser melted AlSi10Mg alloy

Longchao Zhuo [a,*], Zeyu Wang [a], Hongjia Zhang [a], Enhuai Yin [b,*], Yanlin Wang [c,*], Tao Xu [d], Chao Li [b]

[a] School of Materials Science and Engineering, Xi'an University of Technology, Xi'an 710048, China
[b] Xi'an Research Institute of Navigation Technology, China Electronics Technology Group Corporation, Xi'an 710068, China
[c] School of Materials Science and Engineering, University of Science and Technology Beijing, Beijing 100083, China
[d] School of Materials and Chemical Engineering, Xi'an Technological University, Xi'an 710021, China

ARTICLE INFO

*Article history:*
Received 6 August 2018
Received in revised form 6 September 2018
Accepted 19 September 2018
Available online 20 September 2018

*Keywords:*
Selective laser melting
Metals and alloys
AlSi10Mg
Residual stress
X-ray techniques
Mechanical properties

ABSTRACT

In the present work, the model alloy of AlSi10Mg was prepared by selective laser melting, and further annealed by two kinds of heat treatment regimes, i.e. A1 (300 °C/2h+ water quench) and A2 (535 °C/1h + water quench + 190 °C/10 h+ furnace quench). The samples were investigated by XRD, SEM, EBSD, room temperature tensile and nanoindentation tests, to understand the effect of heat treatments on the phase constituents, microstructure, residual stress and mechanical properties of the laser additive manufactured AlSi10Mg alloy. The experimental results showed that, the heat treatment method of A1 is an effective heat treatment regime for eliminating the residual stress and improving the comprehensive mechanical properties for structural applications.



## 1. Introduction

Metal-based additive manufacturing, or three-dimensional (3D) printing, such as selective laser melting (SLM), selective laser sintering and electron beam melting, enables complex geometries, feasible individual design and shorter time to market. This layer by layer powder fusion results in an order of magnitude increase in solidification rate over conventional casting processes, thereby introducing rapidly solidified microstructure and improved mechanical properties [1]. Weldable aluminum alloys based on Al-Si system fabricated by SLM have recently attracted increasing attentions [2]. The limited ductility, the presence of tensile residual stresses caused by the complex thermal history, high defect density and high degree of surface irregularity can adversely affect the structural integrity of SLM parts, which have been tentatively relieved by mechanical (sand blasting and shot peening) or thermal post-treatments [3]. Specifically, it should be noted that the flexible 3D printing for forming special structures such as thin wall components or curving parts, makes the control of residual stress rather crucial for their structure stability and service reliability. Due to the remarkable feasibility, the substrate preheating and post-process treatment of annealing have been widely investigated to remove residual stresses. However, most detailed studies have focused on the effect of T6 heat treatment on SLM Al alloys [3–7]. The T6 regime suitable for conventional fabricated hardenable Al alloys, seems not an optimal candidate for property enhancement after grafted to SLM Al alloys. In this work, two kinds of heat-treatment regime were compared to deeply understand the effect of different heat treatments on microstructure, residual stress and mechanical properties, which would provide a new clue for structural applications of SLM Al alloys.

## 2. Experimental

The SLM processing for fabricating the bulk samples was carried out at room temperature using a SLM 280 HL additive manufacturing system, equipped with a 400 W fiber laser. The information on particle size distribution of the powder feedstock can be found in Fig. S1. Also, the composition (in wt%) of the raw powders was tested by EDS to be 89.1%Al, 10.3% Si, 0.3% Mg and 0.3% Fe, as shown in Fig. S2. Based on a series of preliminary experiments, the following SLM processing parameters of multilayer deposition were chosen: powder layer thickness ($d$) of 0.03 mm, laser beam power ($P$) of 300 W, scan line hatch spacing ($h$) of 0.13 mm, scanning velocity ($v$) of 800 mm/s and laser spot size of 80 μm. The volumetric laser energy densities ($E$) of 62.5 J/mm$^3$ defined by

* Corresponding authors.
*E-mail addresses:* zhuolongchao@xaut.edu.cn (L. Zhuo), yinenhuai@126.com (E. Yin), wangyanlin921@aliyun.com (Y. Wang).

https://doi.org/10.1016/j.matlet.2018.09.109
0167-577X/

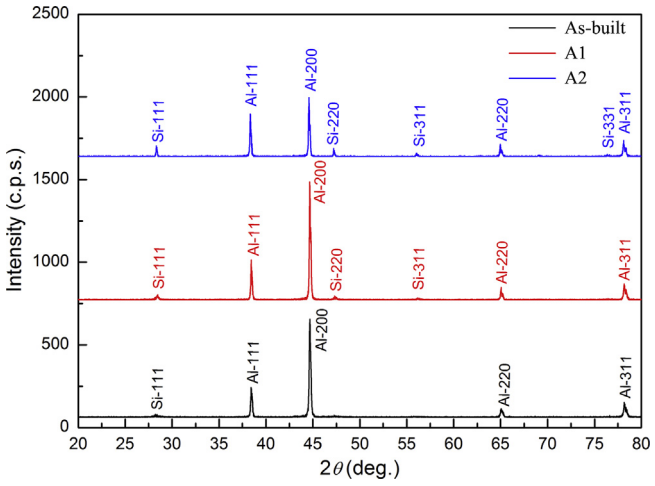


**Fig. 1.** XRD patterns of as-built and heat-treated AlSi10Mg samples. (For interpretation of the references to color in this figure legend, the reader is referred to the web version of this article.)

$E = P/vhd = 96.2$ J/mm$^3$ [8], was used to assess the laser energy input to the powder layer being processed. The oxygen content of less than 100 ppm was kept under an inert argon gas protection, and powder bed temperature was preheated to be 150 °C. For residual stress elimination and ductility enhancement, the samples were also heat-treated under two regimes, i.e. A1 (300 °C/2h + water quench) and A2 (535 °C/1h + water quench + 190 °C/10 h + furnace quench).

XRD measurements for phase analysis have been executed with a MAXima XRD-7000 with Cu-K$\alpha$-radiation under continuous scanning at 3°/min. Residual stress measurement was performed with vanadium filtered Cr-K$\alpha$-radiation with 30 kV and 40 mA and a primary beam diameter of 0.4 mm in $\omega$-mode on the surface layer of the as-built and heat-treated alloys. Electron backscattered diffraction (EBSD) data was acquired using a Zeiss-Merlin SEM with *hkl*-channel 5 system at an acceleration voltage of 20 kV. Characteristic microstructure and mechanical properties were tested along or on the free surface perpendicular to printing Z direction without electrical discharge machining effect from the Al substrate. For phase structure revealing, a solvent containing

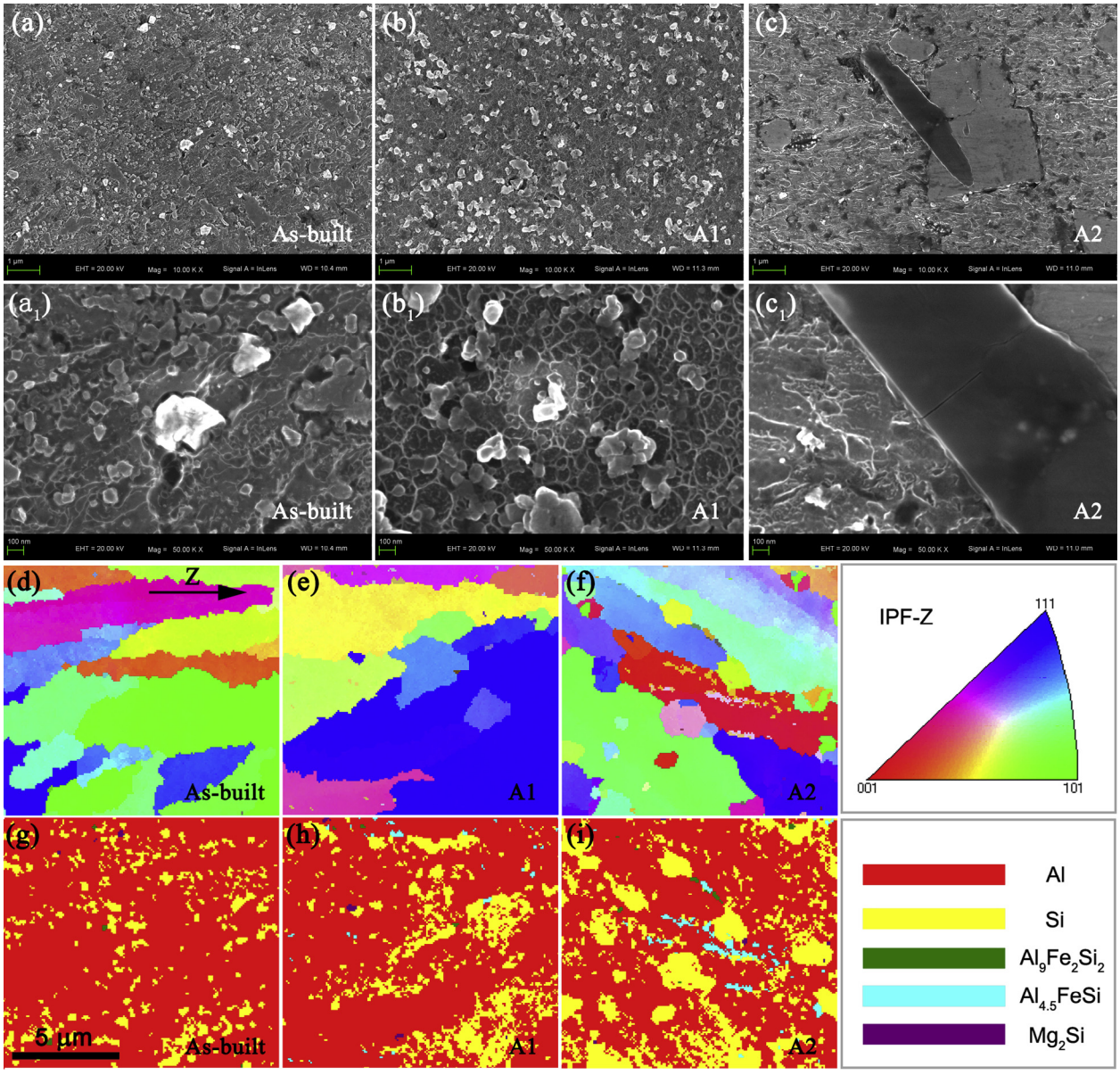


**Fig. 2.** SEM images of as-built (a, $a_1$), A1 (b, $b_1$) and A2 (c, $c_1$) AlSi10Mg samples, as well as the IPF-Z (d–f) and phase distribution maps (g–i) obtained by EBSD. (For interpretation of the references to color in this figure legend, the reader is referred to the web version of this article.)

$HNO_3$ of 25 mL and $H_2O$ of 75 mL was utilized, and the samples were immersed in to the solvent for 40 s at 70 °C, followed by rinse in water. Mechanical properties were determined via tensile testing on Instron-5565 and nano-indentation test on Keysight Nano-indenter G200. Samples with 20 mm gauge length, 6 mm width and 4 mm thick were tested for tensile under a constant strain rate of $5 \times 10^{-4}\ s^{-1}$ at room temperature.

## 3. Results analysis and discussion

XRD phase analysis as shown in Fig. 1 confirmed the existence of α-Al and Si for all three types of samples. For quantitative analysis of binary phase system, the reference intensity ratio (RIR) method is widely adapted due to its feasibility of using *K* values available in ICDD library [9]. Using *K* values of 4.3 and 4.7 and inte-

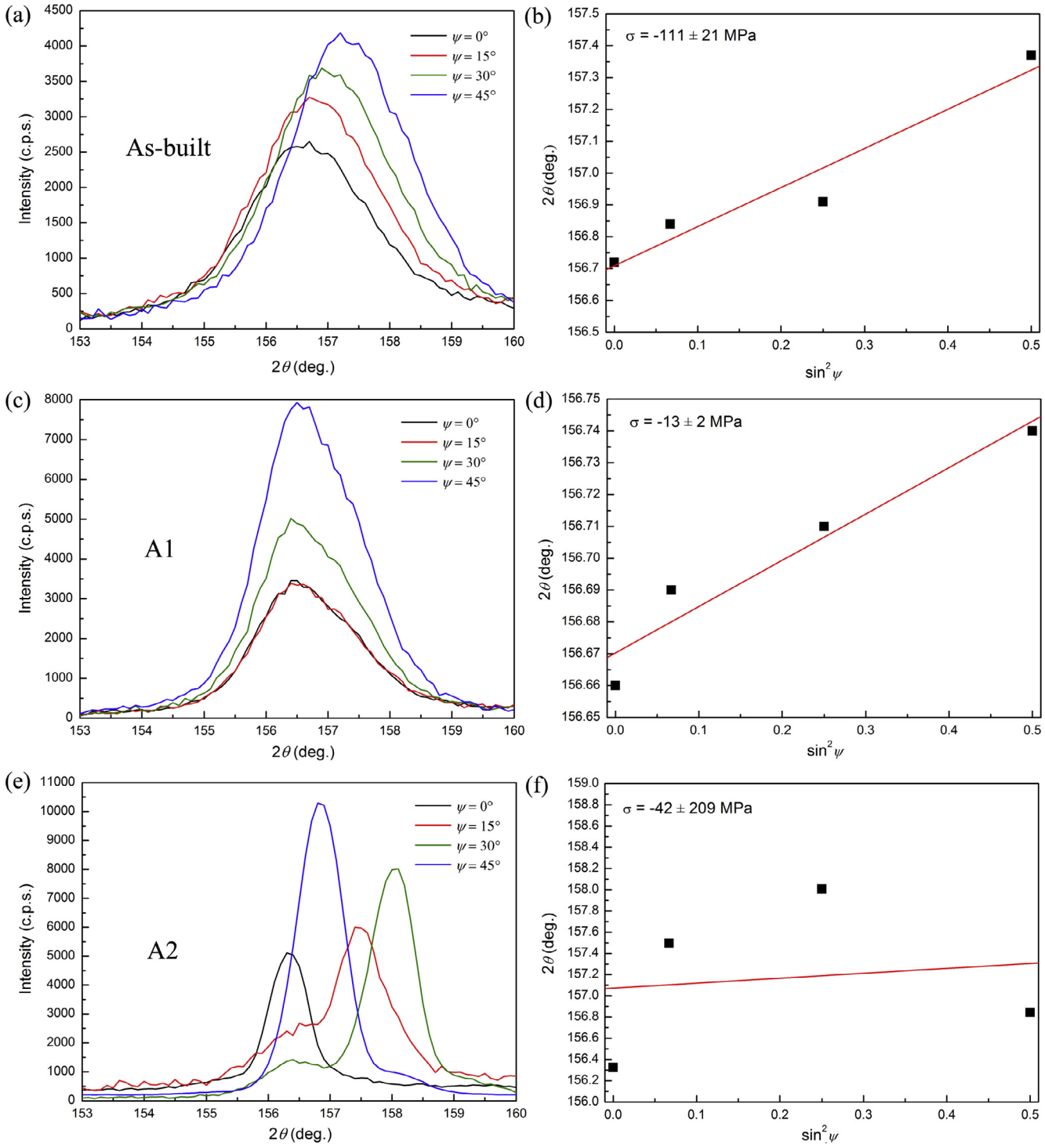


**Fig. 3.** Diffraction peaks for all $\psi$-angles (a, c, e) and $\sin^2\psi$ plots (b, d, f) after residual stress measurements for as-built (a, b), A1 (c, d) and A2 (e, f) heat-treated AlSi10Mg samples. (For interpretation of the references to color in this figure legend, the reader is referred to the web version of this article.)

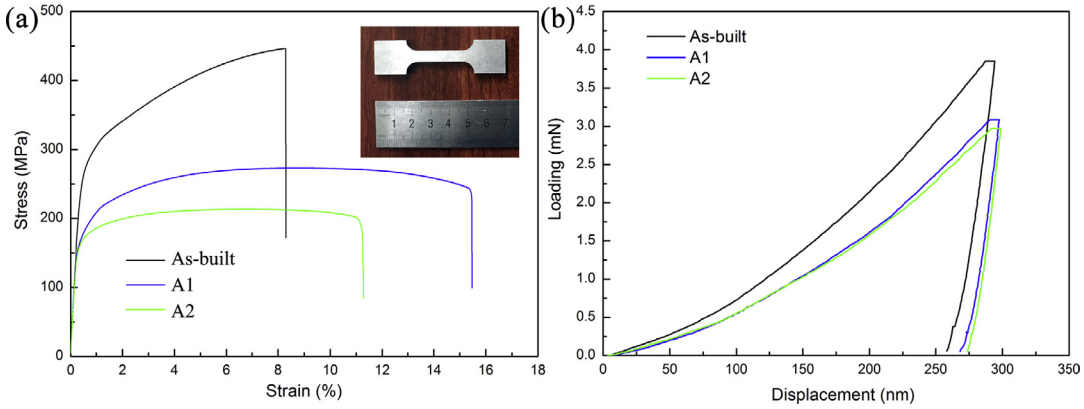


**Fig. 4.** Typical tensile stress-strain curves and nano-indentation results for as-built and heat-treated AlSi10Mg samples. (For interpretation of the references to color in this figure legend, the reader is referred to the web version of this article.)

**Table 1**
Tensile test and nano-indentation results of the as-built and heat-treated samples.

| Samples | Tensile test results | | | | | Nano-indentation results | | |
|---|---|---|---|---|---|---|---|---|
| | $E$ (GPa) | $\sigma_y$ (MPa) | $\sigma_f$ (MPa) | $\psi$ | $\varepsilon$ | Stiffness (kN/m) | $E$ (GPa) | Hardness (GPa) |
| As-built | 74.38 | 270.01 | 446.28 | 9.09% | 8.09% | 152.69 | 98.21 | 2.098 |
| A1 | 78.43 | 169.90 | 273.18 | 31.98% | 15.27% | 164.57 | 103.67 | 1.610 |
| A2 | 76.43 | 164.19 | 213.65 | 24.51% | 11.08% | 160.04 | 99.38 | 1.456 |

gral intensities for respective α-Al and Si, the weight percentage of α-Al and Si were calculated to be respective 97.2% and 2.8% for as-built sample; 94.3% and 5.7% for A1 sample; 89.9% and 10.1% for A2 sample. This indicated the gradual precipitation or coarsening of Si from supersaturated α-Al, which can be seen from the SEM images of the etched samples (Fig. 2(a–c)). Besides, due to the detection limit of X-ray diffraction, local diffraction from Kikuchi patterns in EBSD can reveal more detailed microstructural information, as shown in Fig. 2(d–i). Compared with the supersaturated α-Al exerting strong solution strengthening effect in as-built sample, brittle intermetallic phases of $Al_9Fe_2Si_2$ and $Al_{4.5}FeSi$ precipitated from the A1 and A2 samples, contributing to a detrimental effect on its mechanical properties.

The measured {2 2 2} diffraction peaks of α-Al under different $\psi$ angles of 0°, 15°, 30° and 45° are shown in Fig. 3(a, c, e) and the resulting $\sin^2\psi$ plots [10] are given in Fig. 3(b, d, f). The linear regression of the data sets gave normal residual stress of −111 ± 21 MPa for as-built sample, −13 ± 2 MPa for A1 sample and −42 ± 209 MPa for A2 sample. The sign for negative number stands for its essence of compressive stress, which indicates an excellent fatigue property [11]. It can be also noticed that the as-built and A1 samples presented a well linear fitting of $2\theta$-$\sin^2\psi$, indicating the condition of plane stress; while for A2 sample, the 3D complex stress state due to stress gradient or coarsened grains made an obvious fitting deviation [9]. It can be thereby concluded that the heat treatment method of A1 can effectively eliminate the residual stress of the as-built AlSi10Mg alloy, reserving the size stable enough for structural application.

From the tensile test and nanoindentation results in Fig. 4 and Table 1, it can be seen that the application of SLM with additional A1 heat treatment would result in a more reliable mechanical behavior with engineering-required plasticity of no less than 10% while keeping a relatively high strength of 273.18 MPa. The relatively smaller Young's moduli calculated from the tensile test results compared to the rather local values obtained from nano-indentation tests, is considered to be ascribed to the overall effect such as porosity of the whole sample during tensile tests. This also indicates a possible potential enhancement by further processing parameter optimization, which will be carried out in our future work. On the other hand, the fatigue and wear resistant properties of the samples reported here could be further enhanced or tailored by other post-treatments such as impulse electron beam and shot peening [3,12–14] after the post-treatment of annealing. For assessment of the performance of SLM parts for structural applications, under static loading environment, the SLM parts after A1 heat treatment indicates their structure stability and service reliability for forming special structures such as thin wall components or curving parts; while considering cyclic loading state, the as-built parts with larger compressive residual stress of −111 MPa obtained from the current processing-parameters would exhibit an improved fatigue performance, which will be investigated experimentally in details in our future work.

## 4. Conclusions

In this work, the A1 method of 300 °C/2h + water quench has been determined to be an effective heat treatment regime for eliminating the residual stress and improving the comprehensive mechanical properties of SLM AlSi10Mg alloy. The residual stress of the A1 sample was reduced to be −13 MPa from previous −111 MPa in as-built state; Meanwhile, the A1 sample exhibited optimized tensile properties of high strength of 273.2 MPa and reliable plasticity of 15.3%.

## Acknowledgement

The authors would like to acknowledge the financial support of the National Natural Science Foundation of China (No. 51604223).

## Appendix A. Supplementary data

Supplementary data to this article can be found online at https://doi.org/10.1016/j.matlet.2018.09.109.

## References


[1] J.H. Martin, B.D. Yahata, J.M. Hundley, J.A. Mayer, T.A. Schaedler, T.M. Pollock, 3D printing of high-strength aluminium alloys, Nature 549 (2017) 365–370.

[2] Y. Ding, J.A. Muniz-Lerma, M. Trask, S. Chou, A. Walker, M. Brochu, Microstructure and mechanical property considerations in additive manufacturing of aluminum alloys, MRS Bullet. 41 (2016) 745–751.

[3] S. Bagherifard, N. Beretta, S. Monti, M. Riccio, M. Bandini, M. Guagliano, On the fatigue strength enhancement of additive manufactured AlSi10Mg parts by mechanical and thermal post-processing, Mater. Design 145 (2018) 28–41.

[4] T. Kimura, T. Nakamoto, Microstructure and mechanical properties of Al-10% Si-0.4%Mg fabricated by selective laser melting, J. Jpn. Soc. Powder Metall. 61 (2014) 531–537.

[5] N.T. Aboulkhair, I. Maskery, C. Tuck, I. Ashcroft, N.M. Everitt, The microstructure and mechanical properties of selectively laser melted AlSi10Mg: the effect of a conventional T6-like heat treatment, Mater. Sci. Eng. A 667 (2016) 139–146.

[6] J. Fiocchi, A. Tuissi, P. Bassani, C.A. Biffi, Low temperature annealing dedicated to AlSi10Mg selective laser melting products, J. Alloy. Compd. 695 (2017) 3402–3409.

[7] L. Zhou, A. Mehta, E. Schulz, B. McWilliams, K. Cho, Y. Sohn, Microstructure, precipitates and hardness of selectively laser melted AlSi10Mg alloy before and after heat treatment, Mater. Charact. (2018), https://doi.org/10.1016/j.matchar.2018.04.022.

[8] D.D. Gu, W. Meiners, K. Wissenbach, R. Poprawe, Laser additive manufacturing of metallic components: materials, processes and mechanisms, Int. Mater. Rev. 57 (2012) 133.

[9] S. Hillier, Accurate quantitative analysis of clay and other minerals in sandstones by XRD: comparison of a Rietveld and a reference intensity ratio (RIR) method and the importance of sample preparation, Clay Miner. 35 (2000) 291–302.

[10] G.S. Schajer, Practical Residual Stress Measurement Methods, John Wiley & Sons, 2013.

[11] K.Y. Zhu, C.H. Jiang, V. Ji, Surface layer characteristics of CNT/Al-Mg-Si alloy composites treated by stress peening, Surf. Coat. Technol. 317 (2017) 10–16.

[12] A.D. Pogrebnjak, Y.N. Tyurin, Modification of material properties and coating deposition using plasma jets, Phys. Usp. 48 (5) (2005) 487–514.

[13] A.D. Pogrebnjak, S.M. Ruzimov, D.L. Alontseva, P. Żukowski, C. Karwat, C. Kozak, M. Kolasik, Structure and properties of coatings on Ni base deposited using a plasma jet before and after electron a beam irradiation, Vacuum 81 (2007) 1243–1251.

[14] S. Bagherifard, D.J. Hickey, S. Fintová, F. Pastorek, I. Fernandez-Pariente, M. Bandini, T.J. Webster, M. Guagliano, Effects of nanofeatures induced by severe shot peening (SSP) on mechanical, corrosion and cytocompatibility properties of magnesium alloy AZ31, Acta Biomater. 66 (2018) 93–108.